HHS Public Access

Author manuscript

Neuroimage. Author manuscript; available in PMC 2018 November 01.

Published in final edited form as:

Neuroimage. 2017 November 01; 161: 261–270. doi:10.1016/j.neuroimage.2017.08.045.

Neuroanatomical Foundations of Delayed Reward Discounting Decision Making

Max M. Owens[a], **Joshua C. Gray**[a,b], **Michael T. Amlung**[c], **Assaf Oshri**[d], **Lawrence H. Sweet**[a,e], and **James MacKillop**[a,c,e]

[a]Department of Psychology, University of Georgia, 125 Baldwin Street, Athens, GA 30602

[b]Center for Alcohol and Addiction Studies, Brown University, Providence, RI 02912, USA

[c]Peter Boris Centre for Addiction Research, St. Joseph's Healthcare Hamilton/ McMaster University, 100 West 5th Street, Hamilton, ON L8P 3R2, Canada

[d]College of Family and Consumer Sciences, University of Georgia, 403 Sanford Dr., Athens, GA 30602, USA

[e]Department of Psychiatry and Human Behavior, Brown University, Box G-A1, Providence, Rhode Island 02912

Abstract

Resolving tradeoffs between smaller immediate rewards and larger delayed rewards is ubiquitous in daily life and steep discounting of future rewards is associated with several psychiatric conditions. This form of decision-making is referred to as delayed reward discounting (DRD) and the features of brain structure associated with DRD are not well understood. The current study characterized the relationship between gray matter volume (GMV) and DRD in a sample of 1038 healthy adults (54.7% female) using cortical parcellation, subcortical segmentation, and voxelwise cortical surface-based group analyses. The results indicate that steeper DRD was significantly associated with lower total cortical GMV, but not subcortical GMV. In parcellation analyses, less GMV in 20 discrete cortical regions was associated with steeper DRD. Of these regions, only GMV in the middle temporal gyrus (MTG) and entorhinal cortex (EC) were uniquely associated with DRD. Voxelwise surface-based analyses corroborated these findings, again revealing significant associations between steeper DRD and less GMV in the MTG and EC. To inform the roles of MTG and EC in DRD, connectivity analysis of resting state data (N=1003) using seed regions from the structural findings was conducted. This revealed that spontaneous activity in the MTG and EC was correlated with activation in the ventromedial prefrontal cortex, posterior cingulate cortex, and inferior parietal lobule, regions associated with the default mode network, which involves prospection, self-reflective thinking and mental simulation. Furthermore, meta-analytic co-activation analysis using Neurosynth revealed a similar pattern across 11,406 task-

Corresponding Author: James MacKillop, PhD, Peter Boris Centre for Addictions Research, St. Joseph's Healthcare Hamilton, West 5th Campus/McMaster University, 100 West 5th Street, Hamilton, ON L8P 3R2, Canada, jmackill@mcmaster.ca.

fMRI studies. Collectively, these findings provide robust evidence that morphometric characteristics of the temporal lobe are associated with DRD preferences and suggest it may be because of their role in mental activities in common with default mode activity.

Keywords

Delayed Reward Discounting; MRI; Morphometry; Gray Matter; Behavioral Economics

1. INTRODUCTION

Delayed reward discounting (DRD) refers to a person's preferences for smaller immediate rewards versus larger delayed rewards (i.e., how much a reward is discounted by virtue of its delay in time) (Bickel and Marsch, 2001; Madden and Bickel, 2009). Steep discounting of future rewards is considered a form of impulsivity and has been associated with a variety of different behaviors in normative samples, such as credit card debt (Meier and Sprenger, 2010) and completing regular health screenings (Bradford, 2010). Furthermore, precipitous DRD has been consistently associated with psychiatric disorders such as substance use disorders, gambling disorder, and attention deficit hyperactivity disorder (Amlung et al., 2016b; Jackson and MacKillop, 2016; MacKillop et al., 2011; Reynolds, 2006).

Two fMRI meta-analyses suggest that neural networks involved in cognitive control (e.g., dorsolateral prefrontal cortex, anterior cingulate cortex), valuation of reward (e.g., ventral striatum, orbitofrontal cortex, insula, ventral tegmental area), and self-reflective and future oriented thought (e.g., medial prefrontal cortex, posterior cingulate, tempoparietal junction, lateral and medial temporal lobe; referred to as the default mode network (DMN)) are activated by completing DRD tasks (Carter et al., 2010; Wesley and Bickel, 2014). However, in contrast to the relatively numerous fMRI studies on DRD, there have been surprisingly few studies the relationship of brain structure with DRD. One modestly-sized study reported that DRD was associated with GMV in the ventromedial prefrontal cortex, the anterior cingulate, and the ventral striatum (Cho et al., 2013). This latter association was reported also in a subsequent study investigating only subcortical regions of the brain (Tschernegg et al., 2015). However, two other studies both found associations with the lateral prefrontal cortex, but not the medial prefrontal cortex (Bjork et al., 2009; Mohammadi et al., 2015). The largest study to date found DRD to be associated with GMV in the frontal pole, dorsolateral prefrontal cortex, medial orbitofrontal cortex, parahippocampal gyrus, striatum, temporal pole, precuneus, and precentral gyrus (Wang et al., 2016). Collectively, these initial studies suggest the brain regions in which structure is associated with DRD are those involved in subjective reward valuation (striatum, insula), self-reflective and prospective thought (DMN; medial frontal cortex, posterior cingulate, lateral temporal lobe), and cognitive control (dorsolateral frontal cortex, anterior cingulate cortex).

However, there are a number of inconsistencies across studies and limitations to the literature in general. To start, there has been limited investigation of whether aggregated neurostructural indices, such as total cortical or total subcortical GMV, are related to DRD. Instead, most studies have exclusively focused on *a priori* brain regions that are based on

functional magnetic resonance imaging (fMRI) studies and do not consider the whole brain. This means that there may be other regions that are as important (or more) but are missed. In addition, because of high levels of correlation among cortical regions, *a priori* regions may be artifactually implicated because of interdependence with other unexamined regions, creating false positives. Additionally, the majority of previous studies have only investigated regions defined by an atlas, meaning that there may be relationships of brain structure and DRD that don't fit neatly within these frameworks. Finally, the vast majority of studies to date have been relatively small. Given the increasing acceptance of the potential pitfalls of small sample sized neuroimaging studies (Button et al., 2013), there is clearly a need to address these issues and systematically examine the morphometric correlates of DRD.

The goal of the current study was address a number of these limitations in a large cohort of healthy adults (N = 1038). Using data from the Human Connectome Project (Van Essen et al., 2013a) and a method that models boundaries between gray and white matter throughout the brain, we employed two strategies to characterize the relationship between GMV and DRD. The first strategy used cortical parcellation and subcortical segmentation, first examining total cortical and subcortical GMV in relation to DRD and then exploring neurostructural regions defined by the Desikan atlas, which putatively reflect discrete areas of structural specialization. The second strategy used a voxelwise cortical surface analysis to test associations between GMV in individual voxels and DRD. The two strategies were considered complementary, as the cortical parcellation/subcortical segmentation approach emphasizes regional specialization, whereas the voxelwise approach is atheoretical and makes no assumptions about discrete structural subunits. Together, the two strategies balance the respective benefits and costs, and permit identifying both converging and diverging findings across methodologies. In addition to these primary aims, two follow-up strategies were used to inform the roles of the implicated regions: examination of the patterns of functional connectivity during resting state and generation of a co-activation meta-analysis from other fMRI studies.

2. RESULTS

2.1 Cortical Parcellation and Subcortical Segmentation Analyses

In all instances of significant associations between gray matter volume (GMV) and mean area under the curve for both discounting tasks (mAUC, the primary metric of DRD used; see Methods, section 4.2; note that smaller AUC reflects more impulsive DRD), the relationship between GMV and AUC was positive, indicating that higher levels of GMV were associated with less steep DRD (i.e., more AUC, lower impulsivity). Partial correlations, incorporating demographic covariates, between total cortical gray and total subcortical GMV with mAUC indicated that mAUC was associated with total cortical GMV (r = .124, p = 6E-5; scatterplot in SI Figure 1), but not total subcortical GMV (r = −.010, p = .748). To confirm the lack of association between subcortical GMV and mAUC extended to individual regions (i.e., prevent type II error), we also tested the association of GMV with mAUC in each subcortical region using partial correlations without multiple comparison correction (SI Table 1). No significant associations were found between mAUC and any subcortical regions (all raw/uncorrected p-values > .05).

For completeness, when these analyses were completed with the two individual indices of DRD, area under the curve for $200 (AUC200) and area under the curve for $40,000 (AUC40K), the same general results were found. Both AUC200 and AUC40K were associated with total cortical GMV ($ps \leq .001$) and neither was associated with total subcortical GMV ($ps > .05$). Additionally, neither AUC200 nor AUC40K were associated with any individual subcortical region (all p-values > .05).

Significant partial correlations between cortical parcellation regions and mAUC following FDR correction are listed in Table 1 (associations between all regions and mAUC are listed in SI Table 2). AUC200 and AUC40K were associated with similar regions; regions associated with these indices and associated statistics can be found in SI Table 3. Effect sizes were slightly larger for AUC200 though the same general pattern of regions emerged as significant in both analyses.

In order to determine which regions contributed uniquely to DRD, regression analysis was completed for significant regions in partial correlations. Specifically, regions surviving FDR correction were added to a single regression model of age, sex, income, and intracranial volume to identify regions that were uniquely associated with mAUC. Regions were entered simultaneously and those uniquely predicting mAUC were retained. To evaluate the risk for multicollinearity within the regression models, bivariate correlations were conducted on the five sets of regions which were bilaterally related to mAUC (i.e., bilateral MTG, EC, precentral gyrus, inferior temporal gyrus, lateral orbitofrontal cortex). These revealed large and significant associations between right and left hemisphere in these regions (rs=.57–.86, $ps < .001$; exact correlations reported in SI Table 4). As a result, bilateral regions were consolidated (i.e., summed) to avoid multicollinearity (the consolidated regions are henceforth referred to as bilateral [region name]).

In the regression, only bilateral MTG and bilateral EC were uniquely associated with mAUC (Table 2). An intermediate model that includes the other regions from partial correlations is provided in supplemental materials (SI Table 5). The final model, which included bilateral MTG and bilateral EC (and covariates), accounted for 7.7% of the total variance in DRD; partial regression scatterplots between AUC and both regions are in Figure 1 (including sex, age, income and total intracranial volume in the models). Also of note, bilateral MTG ($\beta = .21$, $t = 3.62$, $p = 8E\text{-}4$) and bilateral EC ($\beta = .16$, $t = 4.34$, $p = 6E\text{-}5$) remained uniquely and significantly associated with mAUC when Total Cortical GMV was added to a follow-up model and the addition of total cortical GMV did not improve the model ($R^2\Delta = 0.000$, $p = .87$). Collectively, the regression results indicate that GMV in the bilateral MTG and bilateral EC accounts for unique variance in mAUC beyond GMV in other regions and GMV throughout the cortex. They also indicate that no other region, nor overall cortical GMV, accounted for additional variance in mAUC beyond bilateral MTG or bilateral EC. Bilateral MTG and bilateral EC were also the only unique predictors for AUC200 and AUC40K (SI Table 6).

2.2 Voxelwise Cortical Surface Analysis

Clusters in which GMV was significantly associated with mAUC at clusterwise $p < .05$ are presented in Table 3 and displayed in in Figure 2. These included clusters in the left MTG,

left lingual gyrus, left EC, left lateral occipital cortex, right fusiform gyrus, right EC, right precentral gyrus, and two clusters in the right MTG. Similar clusters were found for AUC200 while only two clusters in the MTG were associated with AUC40,000 (SI Table 7 and SI Figure 2).

2.3 Resting State Functional Connectivity Analysis

To better understand the role of the morphometric regions that were uniquely associated with mAUC (MTG and EC), resting state functional connectivity of these regions was examined (Figure 2). Seeds for the MTG and EC, denoted by white spheres, were chosen based on the coordinates of peak significance in the regions from the voxelwise cortical surface analysis of mAUC and GMV. Maps of voxelwise time-course correlations with the seeds in the MTG (panels A and B) showed strong positive correlation between the MTG and the medial prefrontal cortex, the posterior cingulate cortex, and inferior parietal lobule, as well as the medial temporal lobe (including the EC). These regions are considered key nodes of the DMN. Negative correlation with the MTG was demonstrated in regions associated with cognitive control including the lateral prefrontal cortex, the supplementary motor area, and the angular gyrus. Similarly, maps for the seeds in the EC (panels C and D) also showed strong positive correlation between the EC and the medial prefrontal cortex, the posterior cingulate cortex, and inferior parietal lobule, as well as the MTG. Negative correlation with the EC was also demonstrated in regions associated with cognitive control including the lateral prefrontal cortex, the supplementary motor area, and the angular gyrus, as well as the precuneus.

3.4 Neurosynth Co-activation Meta-analysis

Finally, to leverage existing data to better understand the association between MTG and EC, task co-activation meta-analyses were completed in Neurosynth. Here, the patterns of co-activation with the seeds used previously for MTG and EC were similar to those found in the resting state functional connectivity analysis of these regions (Figure 3). The MTG seeds showed co-activation with medial prefrontal cortex, the posterior cingulate cortex, and the inferior parietal lobule, as well as the medial temporal lobe, including the EC. Again, these regions are typically considered part of the DMN. The EC seeds also showed co-activation with the medial prefrontal cortex, the posterior cingulate cortex, and the inferior parietal lobule, as well as the lateral temporal lobe including the MTG.

3. DISCUSSION

The goal of this study was to investigate the neurostructural features of the brain that are associated with DRD preferences using both cortical parcellation/subcortical segmentation and total cortical surface area voxelwise approaches. Results of the parcellation analyses indicated associations of DRD with total cortical GMV and GMV in specific focal cortical regions. DRD was associated with GMV in 20 cortical regions including bilaterally in the MTG and EC. However, unique variance in DRD was only predicted by bilateral MTG and EC. Voxelwise cortical surface analyses converged with the parcellation findings, indicating associations between DRD and GMV in bilateral MTG and EC, but also implicating the precentral gyrus, fusiform gyrus, lingual gyrus, and lateral occipital cortex. Follow-up

analyses exploring resting fMRI functional connectivity and task fMRI co-activation between the coordinates of the MTG and EC that were most associated with DRD indicated that these regions are highly (positively) correlated with neural activity in the medial prefrontal cortex, posterior cingulate cortex, and inferior parietal lobule, both at rest and during a variety of tasks. Collectively, these regions are considered key nodes of the DMN (Buckner et al., 2008).

In terms of the specific brain regions whose GMV was found to be associated with DRD, this study's findings that the regions most strongly and uniquely associated with DRD are in the temporal lobe diverge somewhat from the previously reported findings. Studies using with smaller sample sizes have reported relationships between DRD and GMV in different regions, such as prefrontal cortex, insular cortex, and striatum (Bjork et al., 2009; Mohammadi et al., 2015; Tschernegg et al., 2015; Wang et al., 2016). Here, the bilateral orbitofrontal cortex and left insula were associated with mAUC after FDR correction and others of these regions were represented among significant associations in the parcellation analysis (e.g., superior frontal gyrus, frontal pole), but did not survive multiple comparison correction. Critically, however, the variance in DRD accounted for by these regions was not significant beyond that captured by MTG and EC. This suggests that some or all of these prior findings could be due to their collinearity with total cortical GMV or GMV in the MTG or EC. That neither total subcortical GMV nor any specific subcortical regions (particularly the striatum) were even nominally related to DRD was somewhat surprising given prior studies. However, the only prior structural studies to find association between striatal GMV and DRD had considerably smaller sample sizes. It is possible that these findings were false positive or that there is an important unmeasured moderating variable that is responsible for whether DRD is related to striatal GMV. Regarding the numerous fMRI studies findings that activity in the ventral striatum is important to DRD, there is sufficient reason to believe that structure and function do not always overlap, particularly regional GMV and regional task-based activity. For example, a relatively large study (N=156) found no relationship between regional cortical thickness and BOLD fMRI activation in any region of the brain during a working memory task (Squeglia et al., 2013). In addition, other studies directly investigating the relationship between structure and function have found evidence for both convergence and divergence (Honey et al., 2010; Lu et al., 2009).

The most robustly linked regions in the present study and the only ones to predict DRD beyond all other regions and total cortical GMV were the MTG and EC, regions that converge with the largest previous morphometric study (Wang et al., 2016), but have generally not been emphasized in understanding the brain structures associated with DRD. Nonetheless, in prior fMRI meta-analyses on DRD, the MTG was shown be active during DRD tasks across studies, but was not interpreted as part of the key networks identified: the DMN, reward valuation network, and cognitive control networks (Carter et al., 2010; Wesley and Bickel, 2014). However, outside the DRD literature, statistical and theoretical models of the DMN often include the lateral and medial temporal lobe, regions which include the MTG and EC (Andrews-Hanna et al., 2014, 2010; Buckner et al., 2008; Yeo et al., 2011). A recent model of the DMN that provides meta-analytic evidence that the MTG and EC both serve as hubs of DMN subsystems (Andrews-Hanna et al., 2014). According to this model,

the lateral temporal lobe (including MTG) is a part of the dorsal medial subsystem, a component of the DMN that is specifically pertinent to semantic knowledge and self-generated cognitive processes such as theory of mind, and reflection on one's own mental state, preferences, beliefs, desires, and emotions (Andrews-Hanna et al., 2014; Binder et al., 2009; Denny et al., 2012; Lieberman, 2007). The medial temporal lobe (including EC) is a hub of the medial temporal subsystem, a component of the DMN that is essential to autobiographical and episodic memory, simulation of potential future experiences, and construction of mental images (Andrews-Hanna et al., 2014; Bar, 2007; Hassabis et al., 2007; Hassabis and Maguire, 2007; Schacter et al., 2012).

The cognitive functions of these two DMN subsystems can be readily understood in the context of DRD, a process that involves both imagining the future and reflecting on one's own preferences. In other words, these data do not suggest DRD is a default cognitive state, but rather recruits certain cognitive functions in common with default mode processing. This theoretical model of the role the MTG and EC on DRD is supported by the resting state functional connectivity analyses and co-activation meta-analysis that were conducted as part of this study. One hypothesis for why GMV in these temporal lobe regions uniquely is associated with DRD is that they exert a disproportionate impact on the function of the rest of the DMN during DRD. Future studies should explicitly examine how GMV in these areas relates to their activation and connectivity during DRD tasks. More broadly, the current results suggest that these regions' place in the DMN should not be overlooked in future neuroimaging studies of DRD.

Several considerations pertain to the current findings. The study was cross-sectional in design and therefore cannot make claims regarding the causality of the observed relationships. Our assumption is that variation in brain morphology gives rise to the observed DRD, but it is also possible that alternative processes shape a person's DRD preferences and in turn give rise to morphological changes. Future longitudinal studies should address this question. In addition, the functional connectivity and meta-analytic co-activation analyses were exploratory strategies to better understand the primary morphometric findings. They should be taken as empirical conjecture, but not direct evidence for structural characteristics of MTG and EC as determinants of functional activity in DMN. Another consideration pertaining to the healthy population used in the current study is that these results do not speak to how clinical populations with elevations in DRD might differ in brain morphometry. Future studies should attempt to extend these findings in clinical populations and determine if GMV in these regions is associated with the etiology or prognosis of clinical disorders. This is an important question to be addressed given robust evidence that DRD preferences predict treatment response (MacKillop and Kahler, 2009; Sheffer et al., 2014) and highly impulsive DRD appears to be a trans-disease process that is relevant not only to addiction, but other psychiatric disorders (Liu et al., 2012; Urošević et al., 2016; Weller et al., 2014) and health behaviors (Amlung et al., 2016a; Celio et al., 2016; Daugherty and Brase, 2010).

Acknowledging these considerations, it is worth noting that this study had a number of strengths including a large, well-characterized sample and converging evidence from two complementary morphometric approaches and two connectivity/co-activation approaches.

While the fMRI literature on DRD is quite developed, the structural literature is not. Thus, the current study makes a significant contribution to understanding the morphometric correlates of DRD. Addressing the considerable collinearity of GMV among brain regions and conducting voxelwise cortical surface analysis to look for associations between cortical GMV and DRD that are not preordained by a neurostructural atlas, it suggested a clear conclusion that the MTG and EC are uniquely associated with DRD. Further elucidation of the MTG and EC in DRD (and related processes) is clearly warranted in future studies. More broadly, these findings illuminate both the similarities and differences in the regions implicated in a behavioral phenomenon using structural MRI and fMRI.

4. METHODS

4.1 Participants

Structural MRI data were collected from 1113 participants at Washington University in St. Louis over the course of two days as part of the Human Connectome Project between August 2012 and October 2015, and released in full on March 1, 2017. Informed consent was obtained for all participants (consent procedure detailed in (Van Essen et al., 2013a). Participants were 22–35 years old and had no significant history of psychiatric disorder, substance abuse, neurological disorder or damage, cardiovascular disease, or Mendelian genetic disease (e.g., cystic fibrosis). They also did not have any contraindications for receiving an MRI such as metal devices in the body or claustrophobia. For full details of inclusion and exclusion criteria, see (Van Essen et al., 2013b). Of these participants, income for 2 participants was not collected and 8 did not complete the DRD tasks. In addition, adequate task attention and effort was defined as no more than three inconsistent points of indifference (out of 10 possible) on the two DRD tasks combined, resulting in the exclusion of 65 participants (5.8% of total sample). Thus, the primary sample for this study comprised 1038 participants (Table 4).

4.2 Delayed Reward Discounting Task

Two DRD tasks were administered with participants selecting between smaller amounts of money available immediately or larger amounts in the future (e.g., “would you rather have $40 today or $100 in six months)”. Both tasks used an adaptive adjusting-amount approach in which the delay time was held constant and the immediate dollar amount varied on a trial-by-trial basis in accordance with participants’ responding (Estle et al., 2006; Green et al., 2007). One task used a larger delayed amount of $200 and the other used $40,000. For both tasks, participants’ points of indifference were determined for six periods of time: one month, six months, one year, three years, five years, and ten years. These points, defined in units of dollars, represent the immediate amount at which an individual is indifferent between receiving an immediate reward or delay reward (in this case $200 or $40,000) for the given period of time and is conceptualized as the subjective value of a given amount of money at a given delay. For example, a point of indifference of $40 for $100 in 6 months suggests that an individual subjectively values $100 at 40% of the nominal value when it is delayed by six months. In turn, a graphical plot of empirical DRD preferences was generated for each participant using their points of indifference. The plotting of these preferences into a curve permits calculation of the area under that curve using geometry to create trapezoids

between points of indifference and calculating the area of each. The resulting index, area-under-the-curve (AUC), provides a single measure of DRD that is model-free (not reliant on exponential, hyperbolic, or hyperbaloid modelling approaches). Greater area represents less steep DRD and less area represents more steep DRD (Myerson et al., 2001). Greater explanation and justification for the DRD task and index used can be found in the manuscript released by the Human Connectome Project on the behavioral tasks included (Barch et al., 2013).

Each AUC was inspected for distribution and outliers using an outlier threshold of Z = ±4.00 (i.e., four standard deviations above or below the mean) with no outliers being found for either. AUC200 was normally distributed as was AUC40K. DRD performance was highly correlated between the two magnitudes (r = .668, p = 2E-135), so the primary variables was an average of the two was used as a single index of DRD, subsequently referred to as mAUC. mAUC was normally distributed (skewness = .408, kurtosis = −.545) and included no outliers at Z = ±4.00.

4.3 MRI Data Acquisition

High-resolution structural images were collected on a 3T Siemens Skyra scanner (Siemens AG, Erlanger, Germany) with a 32-channel head coil. T1-weighted structural images were acquired with a resolution of 0.7 mm^3 isotropic (FOV = 224x240, matrix = 320x320, 256 sagittal slices; TR = 2400 ms and TE = 2.14 ms). Data were reconstructed and preprocessed using a modified version of the Freesurfer pipeline (Dale et al., 1999; Fischl et al., 2004, 1999a) in FreeSurfer Image Analysis Suite version 5.3 (http://surfer.nmr.mgh.harvard.edu) (Fischl, 2012) and using Chris Rorden's DICOM to NIFTI conversion software (Rorden, 2007). For details of acquisition parameters, reconstruction, and preprocessing of the Human Connectome Project structural MRI data, see (Glasser et al., 2013; Van Essen et al., 2013b).

All structural images were reviewed by a technician immediately following acquisition to ensure scans did not have any significant problems (i.e., artefacts, substantial movement). If problems were found, structural scans were reacquired immediately. Within hours of the initial acquisition, scans were examined by quality control specialists who assessed them for image crispness, blurriness, motion and other artifacts, and accuracy of defacing. Based on these factors, scans were rated on a 1 to 4 scale (poor to excellent). In all cases where structural scans were below 3 (good), new structural scans were reacquired on the participant's second study day. Through this process, all subjects collected had high quality structural imaging data. For full explanation of HCP quality control, see Marcus et al., 2013.

Resting state BOLD fMRI data were collected on the same scanner as structural MRI with a novel multi-band EPI pulse sequence that collects multiple slices simultaneously. Images were acquired with a resolution of 2 mm^3 isotropic (FOV = 208 x 180 x 144, matrix = 104 x 90 , 72 axial slices; TR = 720 ms and TE = 33 ms). Four runs of 15 minutes each were collected in two separate fMRI session with Right-to-Left and Left-to-Right phase encoding done on alternating scans in a counterbalanced fashion. During scans, subjects were asked to lie with eyes open and look at a white fixation cross while thinking of nothing and not falling asleep. Data were spatially and temporally preprocessed in a pipeline designed by Human Connectome Project scientists that utilizes tools from FSL, Freesurfer, and their in-

house software Workbench. From these, a group map is generated allowing for instantaneous correlation of the time-course of any coordinate in the brain with the time-courses of other voxels of the cortical surface, which is available for download on the HCP website (http://www.humanconnectome.org). For full details of acquisition procedures and preprocessing pipeline see (Smith et al., 2013).

4.4 Primary Data Analysis

The principal measure of DRD was mAUC in all analyses, with age, gender, income, and total intracranial volume (ICV) used as covariates in all analyses. These covariates were chosen due to their potentially confounding relationship with DRD and GMV. DRD is known to become less steep (less impulsive) as an individual grows older and GMV is known to decline; men general have steeper DRD than women; income is often related to DRD in monetary tasks as those of lower incomes are often in need of money more immediately for survival reasons; ICV is used to account for differences in GMV due to head and body size. Morphometric analyses were completed using FreeSurfer Image Analysis Suite version 5.3 (http://surfer.nmr.mgh.harvard.edu) (Fischl, 2012) and for all morphometric analyses data was preprocessed using Freesurfer's standard recon-all pipeline (Fischl et al., 2001, 1999b).

4.4.1 Cortical parcellation and subcortical segmentation analyses—Cortical parcellation was used to extract estimates of gray matter volume (GMV) in cortical regions defined by the Desikan atlas (Desikan et al., 2006) and in the cortex as a whole. Subcortical segmentation was used to extract estimates of GMV in subcortical regions and in the subcortical structures as a whole. GMV values for each cortical and subcortical region were then exported into Statistical Package for Social Sciences (SPSS) for analysis with mAUC.

After exporting GMV values for cortical and subcortical structures derived from the atlas, we first conducted the parcellation and segmentation analyses. Covariate-adjusted partial correlations were completed to test the associations of total cortical GMV and total subcortical GMV with mAUC. Then, covariate-adjusted partial correlations were examined between specific brain regions and mAUC (see Supplemental Table 1 for full list of regions). Given the large number of cortical regions in the Desikan atlas ($n = 68$), a two-tailed false discovery rate correction (Benjamini and Hochberg, 1995) of $q = .05$ was implemented to reduce inflation of type I error rate.

To determine which of the regions in from the previous analysis was uniquely associated with DRD (i.e., associated beyond common variance shared among regions) multiple regression was applied to the regions surviving FDR correction in partial correlation analysis. In this regression, age, sex, income, and ICV were entered into the model first. Then the regions associated in previous partial correlations with mAUC were entered simultaneously and those associated with mAUC beyond the other regions were retained in the model to determine the change to R^2 resulting from adding these regions to the model. As a part of this analysis, bivariate correlations were conducted to explore multicollinearity between the five sets of regions which were bilaterally related to mAUC (i.e., bilateral MTG, bilateral EC, precentral gyrus, inferior temporal gyrus, lateral orbitofrontal cortex), revealing

substantial associations between in all bilateral sets (see Supplemental Table 2). As a result, these regions were consolidated (i.e., summed) in the final regression analyses to avoid multicollinearity problems in subsequent multiple regression models.

4.4.2 Voxelwise Cortical Surface Analysis—Subsequently, cortical surface voxelwise analysis was used to assess the relationship of GMV with mAUC voxel-by-voxel in an approach that was atheoretical following the procedure described by Fischl and Dale (Dale et al., 1999; Fischl et al., 1999a). This was done entirely in FreeSurfer with the final output being a brain map of correlations between GMV and mAUC and a table of all clusters of correlation between GMV and mAUC found. This approach allows for the statistical comparison and visualization of volume in analogous regions across subjects using a common space based on the 2D surface of the brain rather than a 3D template of the brain, which is considered to be superior given inherent differences in brain topography from subject to subject. In the first step of this procedure cortical surfaces of the brains of individual subject were divided into voxels using triangular tessellation, with each voxel associated with a specific value representing the GMV at that voxel. Voxels in this approach are triangular in order to map them onto a 2D surface (whereas traditional voxel based morphometry uses 3D square voxels). Then subjects' brains were aligned based on the patterns of cortical surface features (e.g., sulci and gyri) and transformed into a standard space. Then voxel-by-voxel general linear modeling was completed to determine cluster of voxels for which there was a significant correlation between GMV (in mm^3) and mAUC. Clusterwise correction for multiple comparisons was then completed using Monte Carlo simulations (Hagler et al., 2006). In this process, data are tested against a null distribution of maximum cluster size with an initial cluster-forming threshold of $p < .001$. This yields clusters corrected for multiple comparisons based on the total number of comparisons on the surface. Using this method, regions in which GMV was associated with mAUC at a cluster corrected p-value of less than .05 were determined. For further explanation of the interpretation of GMV in voxelwise cortical surface analyses, see Winkler et al., 2012.

4.5 Supplementary Connectivity and Co-Activation Analyses

After completing primary analyses investigating DRD's relationship with regional GMV, two supplementary analyses were conducted to explore the network connectivity of regions in which GMV was uniquely associated with DRD in multiple regression analysis. First, as a means of inferring the functional network to which the relevant regions belonged, functional connectivity analysis was performed on resting state fMRI from the available HCP participants ($N = 1003$). This subsample did not differ demographically from the sample included in GMV analyses (see SI Table 8 for full demographic information). Using the resting state correlation map described above (section 4.3), coordinates of the peak association of mAUC and GMV in the right and left MTG and EC were drawn as seed regions of interest (ROI) that were 6mm in diameter. The correlations of the timecourse of these seed ROIs with the timecourses from each voxel in the cortical surface were then calculated. From this, brain maps were derived showing the functional connectivity of each seed.

Second, to attempt to confirm the networks to which the regions predicting mAUC belonged, the online database Neurosynth (www.neurosynch.org) was used to conduct a large-scale automated meta-analyses of co-activation for the regions in which GMV was found to be uniquely predictive of DRD in multiple regression analyses (Yarkoni et al., 2011). Coordinates of the peak association of mAUC and GMV in the left and right MTG and EC were used as regions of interests (ROIs) in co-activation analysis. Neurosynth was used to conduct meta-analyses of all the fMRI studies in its database for co-activation for within 10mm from the ROIs input. This generated whole brain z-score maps showing the likelihood a voxel co-activated with the ROI. The studies used in this analysis were task fMRI studies and the results, therefore, reflect putative network connectivity during a variety of tasks. This differs from the resting state fMRI analysis which measured co-activation at rest. However, prior research suggests that these two analyses should be comparable as brain networks are thought to represent permanent functional units whose activation patterns hang together in most-to-all circumstances (Yeo et al., 2015). Since Neurosynth is continuously updating, it is worth noting that this analysis was conducted on April 18th, 2017 when Neurosynth had 11,406 studies, and 150,000 brain locations.

Supplementary Material

Refer to Web version on PubMed Central for supplementary material.

Acknowledgments

These data were provided by the Human Connectome Project, WU-Minn Consortium (Principal Investigators: David Van Essen and Kamil Ugurbil; 1U54MH091657) funded by the 16 NIH Institutes and Centers that support the NIH Blueprint for Neuroscience Research; and by the McDonnell Center for Systems Neuroscience at Washington University in St. Louis. The authors are deeply appreciative to the Human Connectome Project for open access to its data. In addition, the work was partially supported by NIH grant P30 DA027827 (LS, JM) and the Peter Boris Chair in Addictions Research (JM). These funding sources were not involved in study design or collection, analysis, and interpretation of the data.

References

Amlung M, Petker T, Jackson J, Balodis I, MacKillop J. Steep discounting of delayed monetary and food rewards in obesity: a meta-analysis. Psychol Med. 2016a; 46:2423–34. DOI: 10.1017/S0033291716000866 [PubMed: 27299672]

Amlung M, Vedelago L, Acker J, Balodis I, Mackillop J. Steep delay discounting and addictive behavior: A meta-analysis of continuous associations. Addiction. 2016b; doi: 10.1111/add.13535

Andrews-Hanna JR, Reidler JS, Sepulcre J, Poulin R, Buckner RL. Functional-anatomic fractionation of the brain's default network. Neuron. 2010; 65:550–562. DOI: 10.1016/j.neuron.2010.02.005 [PubMed: 20188659]

Andrews-Hanna JR, Smallwood J, Spreng RN. The default network and self-generated thought: Component processes, dynamic control, and clinical relevance. Ann N Y Acad Sci. 2014; 1316:29–52. DOI: 10.1111/nyas.12360 [PubMed: 24502540]

Bar M. The proactive brain: using analogies and associations to generate predictions. Trends Cogn Sci. 2007; 11:280–289. DOI: 10.1016/j.tics.2007.05.005 [PubMed: 17548232]

Barch DM, Burgess GC, Harms MP, Petersen SE, Schlaggar BL, Corbetta M, Glasser MF, Curtiss S, Dixit S, Feldt C, Nolan D, Bryant E, Hartley T, Footer O, Bjork JM, Poldrack R, Smith S, Johansen-Berg H, Snyder AZ, Van Essen DC. Function in the human connectome: Task-fMRI and individual differences in behavior. Neuroimage. 2013; 80:169–189. DOI: 10.1016/j.neuroimage.2013.05.033 [PubMed: 23684877]

Benjamini Y, Hochberg Y. Controlling the false discovery rate: a practical and powerful approach to multiple testing. J R Stat Soc. 1995; 57:289–300. DOI: 10.2307/2346101

Bickel WK, Marsch LA. Toward a behavioral economic understanding of drug dependence: delay discounting processes. Addiction. 2001; 96:73–86. DOI: 10.1080/09652140020016978 [PubMed: 11177521]

Binder JR, Desai RH, Graves WW, Conant LL. Where is the semantic system? A critical review and meta-analysis of 120 functional neuroimaging studies. Cereb Cortex. 2009; 19:2767–2796. DOI: 10.1093/cercor/bhp055 [PubMed: 19329570]

Bjork JM, Momenan R, Hommer DW. Delay Discounting Correlates with Proportional Lateral Frontal Cortex Volumes. Biol Psychiatry. 2009; 65:710–713. DOI: 10.1016/j.biopsych.2008.11.023 [PubMed: 19121516]

Bradford WD. The association between individual time preferences and health maintenance habits. Med Decis Making. 2010; 30:99–112. DOI: 10.1177/0272989X09342276 [PubMed: 19675322]

Buckner RL, Andrews-Hanna JR, Schacter DL. The brain's default network: Anatomy, function, and relevance to disease. Ann N Y Acad Sci. 2008; 1124:1–38. DOI: 10.1196/annals.1440.011 [PubMed: 18400922]

Button KS, Ioannidis JPA, Mokrysz C, Nosek BA, Flint J, Robinson ESJ, Munafò MR. Power failure: why small sample size undermines the reliability of neuroscience. Nat Rev Neurosci. 2013; 14:365–76. DOI: 10.1038/nrn3475 [PubMed: 23571845]

Carter RM, Meyer JR, Huettel Sa. Functional neuroimaging of intertemporal choice models: A review. J Neurosci Psychol Econ. 2010; 3:27–45. DOI: 10.1037/a0018046

Celio MA, Mackillop J, Caswell AJ, Mastroleo NR, Kahler CW, Barnett NP, Colby SM, Operario D, Monti PM. Interactive Relationships Between Sex-Related Alcohol Expectancies and Delay Discounting on Risky Sex. Alcohol Clin Exp Res. 2016; 40:638–646. DOI: 10.1111/acer.12988 [PubMed: 26891345]

Cho SS, Pellecchia G, Aminian K, Ray N, Segura B, Obeso I, Strafella AP. Morphometric correlation of impulsivity in medial prefrontal cortex. Brain Topogr. 2013; 26:479–487. DOI: 10.1007/s10548-012-0270-x [PubMed: 23274773]

Dale AM, Fischl B, Sereno MI. Cortical surface-based analysis. I Segmentation and surface reconstruction. Neuroimage. 1999; 9:179–194. DOI: 10.1006/nimg.1998.0395 [PubMed: 9931268]

Daugherty JR, Brase GL. Taking time to be healthy: Predicting health behaviors with delay discounting and time perspective. Pers Individ Dif. 2010; 48:202–207. DOI: 10.1016/j.paid.2009.10.007

Denny B, Kober H, Wager T, Ochsner K. A meta-analysis of functional neuroimaging studies of self and other judgments reveals a spatial gradient for mentalizing in medial prefrontal cortex. J Cogn Neurosci. 2012; 24:1742–1752. DOI: 10.1162/jocn [PubMed: 22452556]

Desikan RS, Segonne F, Fischl B, Quinn BT, Dickerson BC, Blacker D, Buckner RL, Dale AM, Maguire RP, Hyman BT, Albert MS, Killiany RJ. An automated labeling system for subdividing the human cerebral cortex on MRI scans into gyral based regions of interest. Neuroimage. 2006; 31:968–980. DOI: 10.1016/j.neuroimage.2006.01.021 [PubMed: 16530430]

Estle SJ, Green L, Myerson J, Holt DD. Differential effects of amount on temporal and probability discounting of gains and losses. Mem Cognit. 2006; 34:914–928. DOI: 10.3758/BF03193437

Fischl B. FreeSurfer. Neuroimage. 2012; doi: 10.1016/j.neuroimage.2012.01.021

Fischl B, Liu A, Dale AM. Automated manifold surgery: Constructing geometrically accurate and topologically correct models of the human cerebral cortex. IEEE Trans Med Imaging. 2001; 20:70–80. DOI: 10.1109/42.906426 [PubMed: 11293693]

Fischl B, Sereno MI, Dale AM. Cortical Surface-Based Analysis: II: Inflation, Flattening, and a Surface-Based Coordinate System. Neuroimage. 1999a; 9:195–207. DOI: 10.1006/nimg.1998.0396 [PubMed: 9931269]

Fischl B, Sereno MI, Tootell RBH, Dale AM. High-resolution intersubject averaging and a coordinate system for the cortical surface. Hum Brain Mapp. 1999b; 8:272–284. DOI: 10.1002/(SICI)1097-0193(1999)8:4<272::AID-HBM10>3.0.CO;2-4 [PubMed: 10619420]

Glasser MF, Sotiropoulos SN, Wilson JA, Coalson TS, Fischl B, Andersson JL, Xu J, Jbabdi S, Webster M, Polimeni JR, Van Essen DC, Jenkinson M. The minimal preprocessing pipelines for the Human Connectome Project. Neuroimage. 2013; 80:105–124. DOI: 10.1016/j.neuroimage.2013.04.127 [PubMed: 23668970]

Green L, Myerson J, Shah AK, Estle SJ, Holt DD. Do adjusting-amount and adjusting-delay procedures produce equivalent estimates of subjective value in pigeons? J Exp Anal Behav. 2007; 87:337–347. DOI: 10.1901/jeab.2007.37-06 [PubMed: 17575900]

Hagler DJ, Saygin AP, Sereno MI. Smoothing and cluster thresholding for cortical surface-based group analysis of fMRI data. Neuroimage. 2006; 33:1093–1103. DOI: 10.1016/j.neuroimage.2006.07.036 [PubMed: 17011792]

Hassabis D, Kumaran D, Vann SD, Maguire Ea. Patients with hippocampal amnesia cannot imagine new experiences. Proc Natl Acad Sci U S A. 2007; 104:1726–1731. DOI: 10.1073/pnas.0610561104 [PubMed: 17229836]

Hassabis D, Maguire EA. Deconstructing episodic memory with construction. Trends Cogn Sci. 2007; 11:299–306. DOI: 10.1016/j.tics.2007.05.001 [PubMed: 17548229]

Honey CJ, Thivierge JP, Sporns O. Can structure predict function in the human brain? Neuroimage. 2010; doi: 10.1016/j.neuroimage.2010.01.071

Jackson JNS, MacKillop J. Attention deficit hyperactivity disorder and monetary delay discounting: A meta-analysis of case-control studies. Biol Psychiatry Cogn Neurosci Neuroimaging. 2016; doi: 10.1016/j.bpsc.2016.01.007

Lieberman MD. Social cognitive neuroscience: a review of core processes. Annu Rev Psychol. 2007; 58:259–289. DOI: 10.1146/annurev.psych.58.110405.085654 [PubMed: 17002553]

Liu RT, Vassileva J, Gonzalez R, Martin EM. A comparison of delay discounting among substance users with and without suicide attempt history. Psychol Addict Behav. 2012; 26:980–985. DOI: 10.1037/a0027384 [PubMed: 22369220]

Lu LH, Dapretto M, O'Hare ED, Kan E, McCourt ST, Thompson PM, Toga AW, Bookheimer SY, Sowell ER. Relationships between brain activation and brain structure in normally developing children. Cereb Cortex. 2009; 19:2595–2604. DOI: 10.1093/cercor/bhp011 [PubMed: 19240138]

MacKillop J, Amlung MT, Few LR, Ray LA, Sweet LH, Munaf?? MR. Delayed reward discounting and addictive behavior: A meta-analysis. Psychopharmacology (Berl). 2011; 216:305–321. DOI: 10.1007/s00213-011-2229-0 [PubMed: 21373791]

MacKillop J, Kahler CW. Delayed reward discounting predicts treatment response for heavy drinkers receiving smoking cessation treatment. Drug Alcohol Depend. 2009; 104:197–203. DOI: 10.1016/j.drugalcdep.2009.04.020 [PubMed: 19570621]

Madden GJ, Bickel WK. Impulsivity: The Behavioral and Neurological Science of Discounting. 2009

Marcus DS, Harms MP, Snyder AZ, Jenkinson M, Wilson JA, Glasser MF, Barch DM, Archie KA, Burgess GC, Ramaratnam M, Hodge M, Horton W, Herrick R, Olsen T, McKay M, House M, Hileman M, Reid E, Harwell J, Coalson T, Schindler J, Elam JS, Curtiss SW, Van Essen DC. Human Connectome Project informatics: Quality control, database services, and data visualization. Neuroimage. 2013; 80:202–219. DOI: 10.1016/j.neuroimage.2013.05.077 [PubMed: 23707591]

Meier S, Sprenger C. Present-biased preferences and credit card borrowing. Am Econ J Appl Econ. 2010; 2:193–210. DOI: 10.1257/app.2.1.193

Mohammadi B, Hammer A, Miedl SF, Wiswede D, Marco-Pallares J, Herrmann M, Munte TF. Intertemporal choice behavior is constrained by brain structure in healthy participants and pathological gamblers. Brain Struct Funct. 2015; :3157–3170. DOI: 10.1007/s00429-015-1093-9 [PubMed: 26239549]

Reynolds B. A review of delay-discounting research with humans: relations to drug use and gambling. Behav Pharmacol. 2006; 17:651–667. DOI: 10.1097/FBP.0b013e3280115f99 [PubMed: 17110792]

Schacter DL, Addis DR, Hassabis D, Martin VC, Spreng RN, Szpunar KK. The Future of Memory: Remembering, Imagining, and the Brain. Neuron. 2012; doi: 10.1016/j.neuron.2012.11.001

Sheffer CE, Christensen DR, Landes R, Carter LP, Jackson L, Bickel WK. Delay discounting rates: A strong prognostic indicator of smoking relapse. Addict Behav. 2014; 39:1682–1689. DOI: 10.1016/j.addbeh.2014.04.019 [PubMed: 24878037]

Smith SM, Beckmann CF, Andersson J, Auerbach EJ, Bijsterbosch J, Douaud G, Duff E, Feinberg DA, Griffanti L, Harms MP, Kelly M, Laumann T, Miller KL, Moeller S, Petersen S, Power J, Salimi-Khorshidi G, Snyder AZ, Vu AT, Woolrich MW, Xu J, Yacoub E, Uğurbil K, Van Essen DC, Glasser MF. Resting-state fMRI in the Human Connectome Project. Neuroimage. 2013; 80:144–168. DOI: 10.1016/j.neuroimage.2013.05.039 [PubMed: 23702415]

Squeglia LM, McKenna BS, Jacobus J, Castro N, Sorg SF, Tapert SF. BOLD response to working memory not related to cortical thickness during early adolescence. Brain Res. 2013; 1537:59–68. DOI: 10.1016/j.brainres.2013.08.053 [PubMed: 24012876]

Tschernegg M, Pletzer B, Schwartenbeck P, Ludersdorfer P, Hoffmann U, Kronbichler M. Impulsivity relates to striatal gray matter volumes in humans: evidence from a delay discounting paradigm. Front Hum Neurosci. 2015; 9:1–9. DOI: 10.3389/fnhum.2015.00384 [PubMed: 25653611]

Urošević S, Youngstrom EA, Collins P, Jensen JB, Luciana M. Associations of age with reward delay discounting and response inhibition in adolescents with bipolar disorders. J Affect Disord. 2016; 190:649–656. DOI: 10.1016/j.jad.2015.11.005 [PubMed: 26590512]

Van Essen DC, Smith SM, Barch DM, Behrens TEJ, Yacoub E, Ugurbil K. The WU-Minn Human Connectome Project: An overview. Neuroimage. 2013a; 80:62–79. DOI: 10.1016/j.neuroimage.2013.05.041 [PubMed: 23684880]

Van Essen DC, Ugurbil K, Auerbach E, Barch D, Behrens T, Bucholz R, Chang A, Chen L, Corbetta M, Curtiss S, Della Penna S, Feinberg D, Glasser M, Harel N, Heath A, Larson-Prior L, Marcus D, Michalareas G, Moeller S, Oostenveld R, Petersen S, Prior F, Schlaggar B, Smith S, Snyder A, Xu J, Yacoub E. The Human Connectome Project : A data acquisition perspective. Neuroimage. 2013b; 62:2222–2231. DOI: 10.1016/j.neuroimage.2012.02.018.The

Wang Q, Chen C, Cai Y, Li S, Zhao X, Zheng L, Zhang H, Liu J, Chen C, Xue G. Dissociated neural substrates underlying impulsive choice and impulsive action. Neuroimage. 2016; 134:540–549. DOI: 10.1016/j.neuroimage.2016.04.010 [PubMed: 27083527]

Weller RE, Avsar KB, Cox JE, Reid MA, White DM, Lahti AC. Delay discounting and task performance consistency in patients with schizophrenia. Psychiatry Res. 2014; 215:286–293. DOI: 10.1016/j.psychres.2013.11.013 [PubMed: 24388727]

Wesley MJ, Bickel WK. Remember the Future II: Meta-analyses and Functional Overlap of Working Memory and Delay Discounting. Biol Psychiatry. 2014; 75:435–448. DOI: 10.1016/j.biopsych.2013.08.008 [PubMed: 24041504]

Winkler AM, Sabuncu MR, Yeo BTT, Fischl B, Greve DN, Kochunov P, Nichols TE, Blangero J, Glahn DC. Measuring and comparing brain cortical surface area and other areal quantities. Neuroimage. 2012; 61:1428–1443. DOI: 10.1016/j.neuroimage.2012.03.026 [PubMed: 22446492]

Yarkoni T, Poldrack RA, Nichols TE, Van Essen DC, Wager TD. Large-scale automated synthesis of human functional neuroimaging data. Nat Methods. 2011; 8:665–670. DOI: 10.1038/nmeth.1635 [PubMed: 21706013]

Yeo BT, Krienen FM, Eickhoff SB, Yaakub SN, Fox PT, Buckner RL, Asplund CL, Chee MWL. Functional specialization and flexibility in human association cortex. Cereb Cortex. 2015; 25:3654–3672. DOI: 10.1093/cercor/bhu217 [PubMed: 25249407]

Yeo BT, Krienen FM, Sepulcre J, Sabuncu MR, Lashkari D, Hollinshead M, Roffman JL, Smoller JW, Zollei L, Polimeni JR, Fischl B, Liu H, Buckner RL. The organization of the human cerebral cortex estimated by intrinsic functional connectivity. J Neurophysiol. 2011; 106:1125–1165. DOI: 10.1152/jn.00338.2011 [PubMed: 21653723]

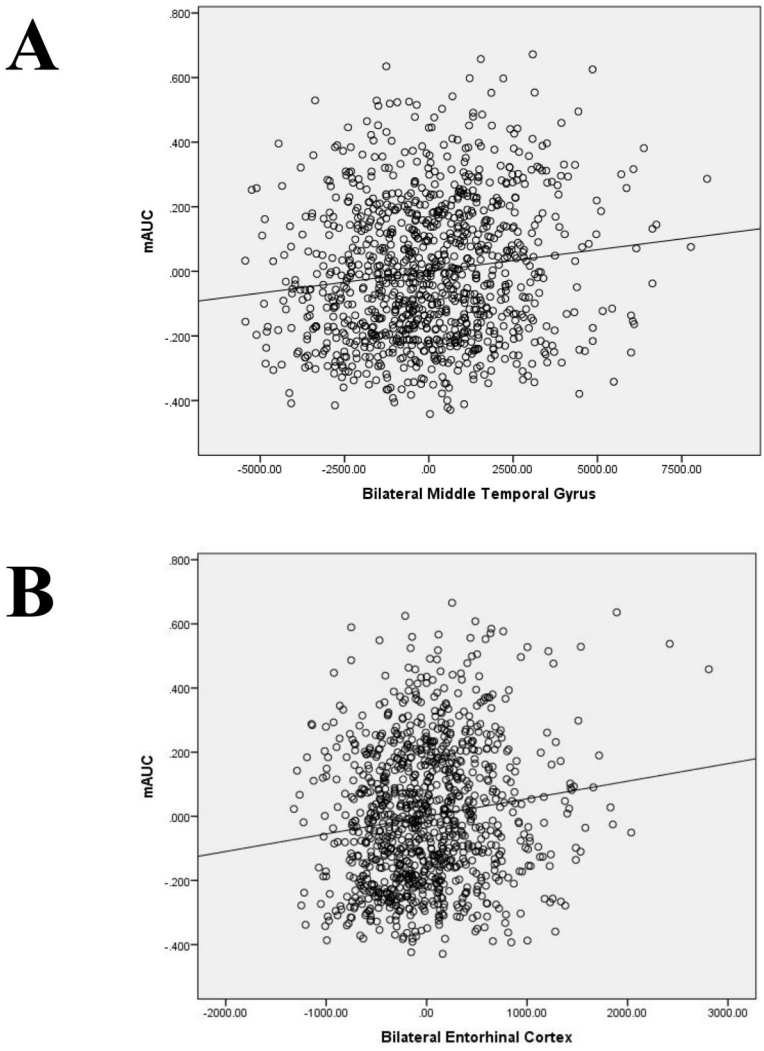

Figure 1.

Partial regressions of mean delayed reward discounting area under the curve in relation to bilateral middle temporal gyrus (Panel A) and bilateral entorhinal cortex (Panel B); sex, age, income and intracranial volume are included in the models.

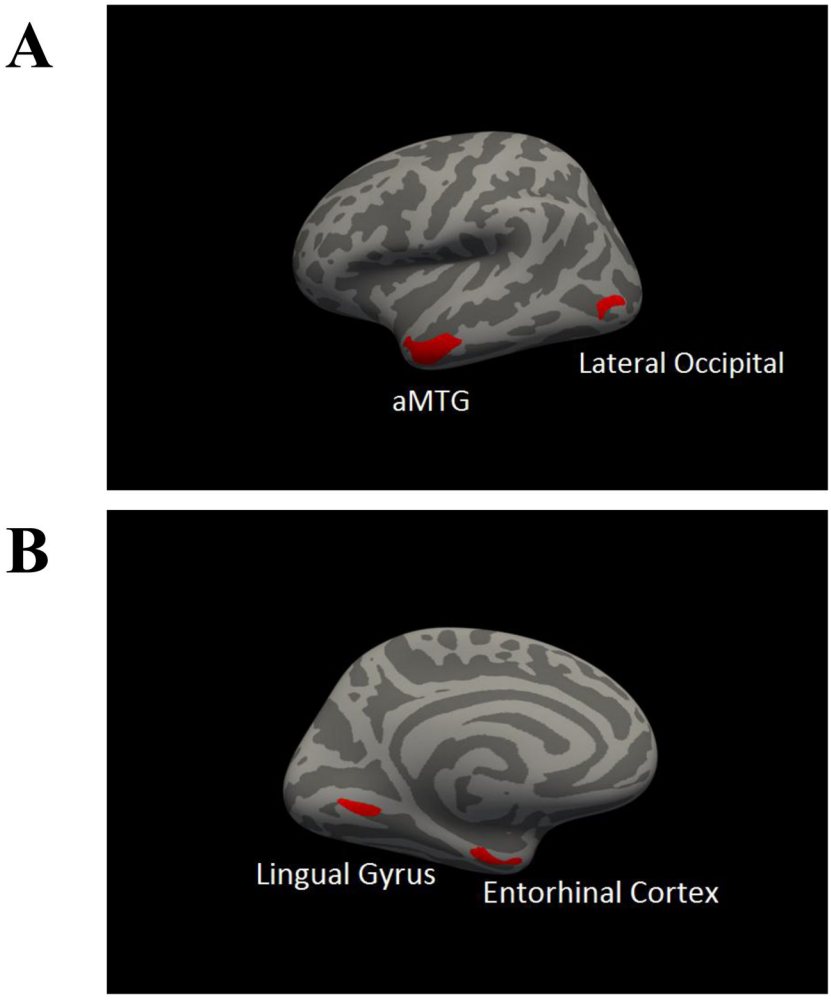

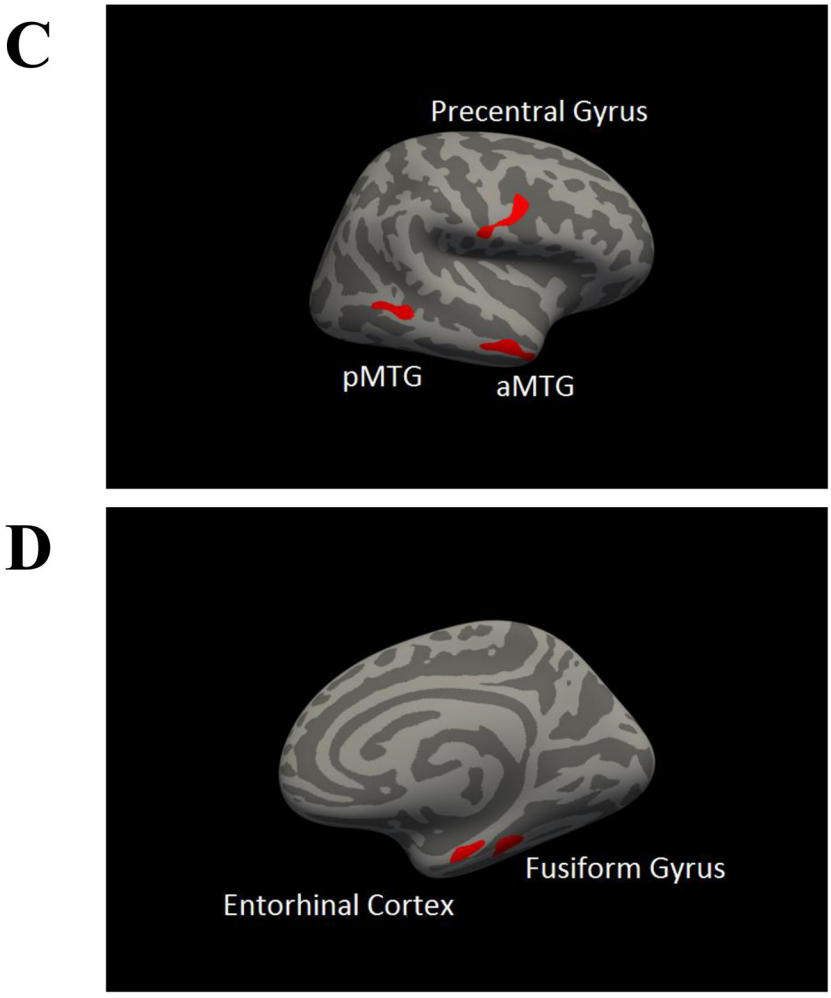

Figure 2.

Whole brain correlation of gray matter volume and area under the curve. All clusters represent a positive correlation of mean area under the curve and regional gray matter volume. Panel A presents a lateral view of the left hemisphere, panel B presents a medial view of left hemisphere, panel C represents lateral view of the right hemisphere, panel D represents medial view of the right hemisphere. aMTG = anterior middle temporal gyrus; pMTG = posterior middle temporal gyrus.

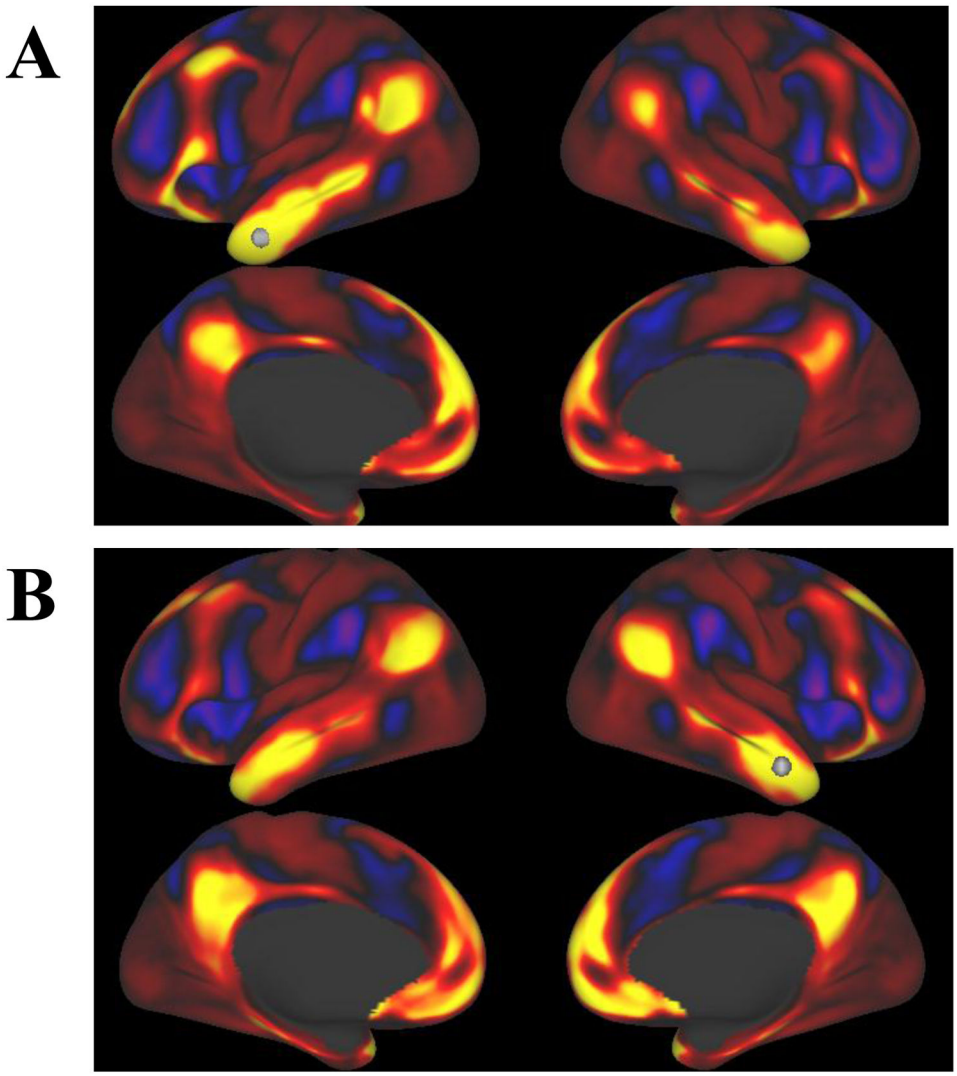

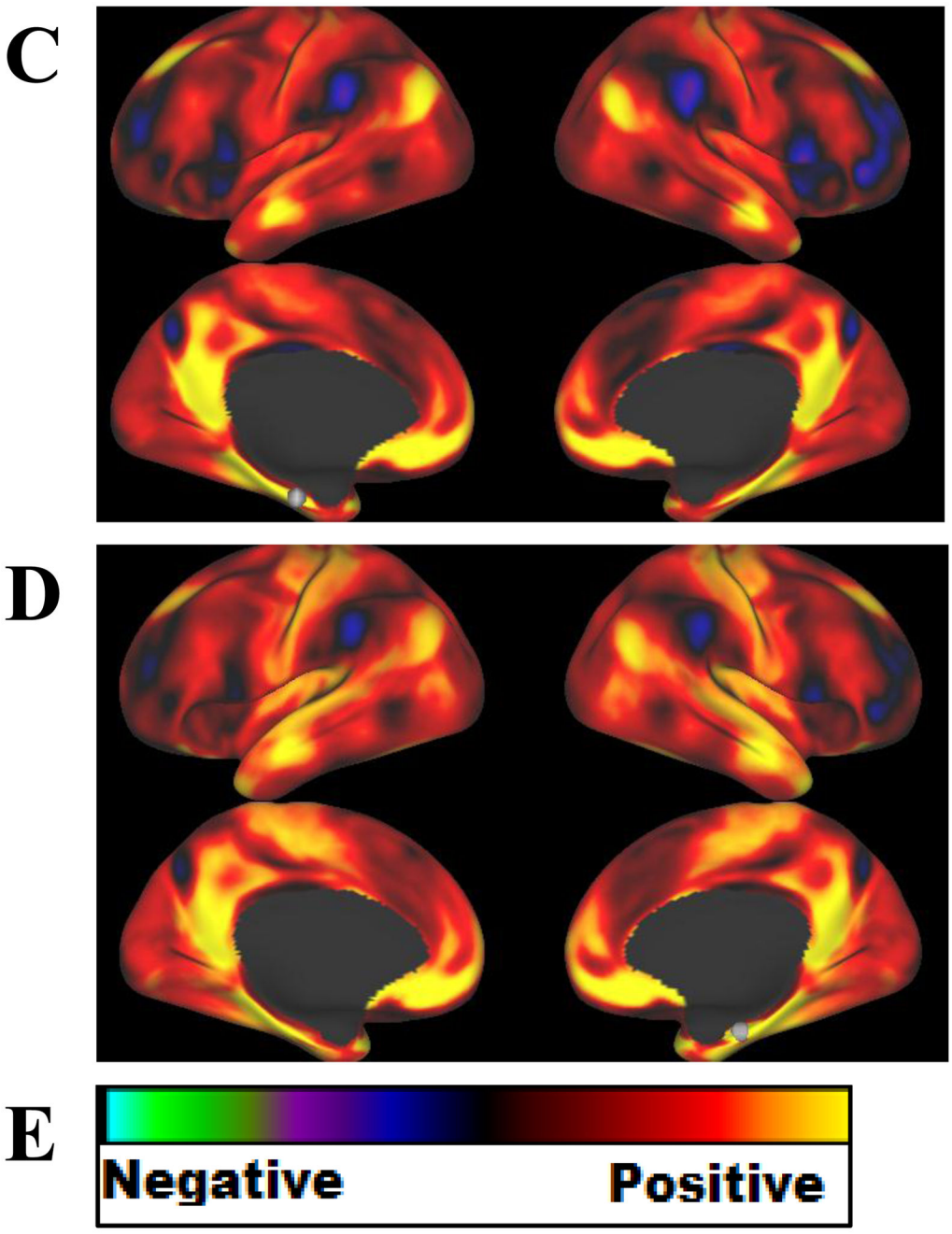

Figure 3.

Resting state functional connectivity for seeds based on the structural analyses in the Human Connectome Project (*N*=1003) total sample. Each image shows a voxelwise correlation of all voxels on the cortical surface (no subcortical regions) with a seed identified from the voxelwise cortical surface analysis of GMV and mAUC (shown as a white sphere). Seeds were A) left middle temporal gyrus B) right middle temporal gyrus C) left entorhinal cortex D) right entorhinal cortex. Panel E displays the color scale used.

A

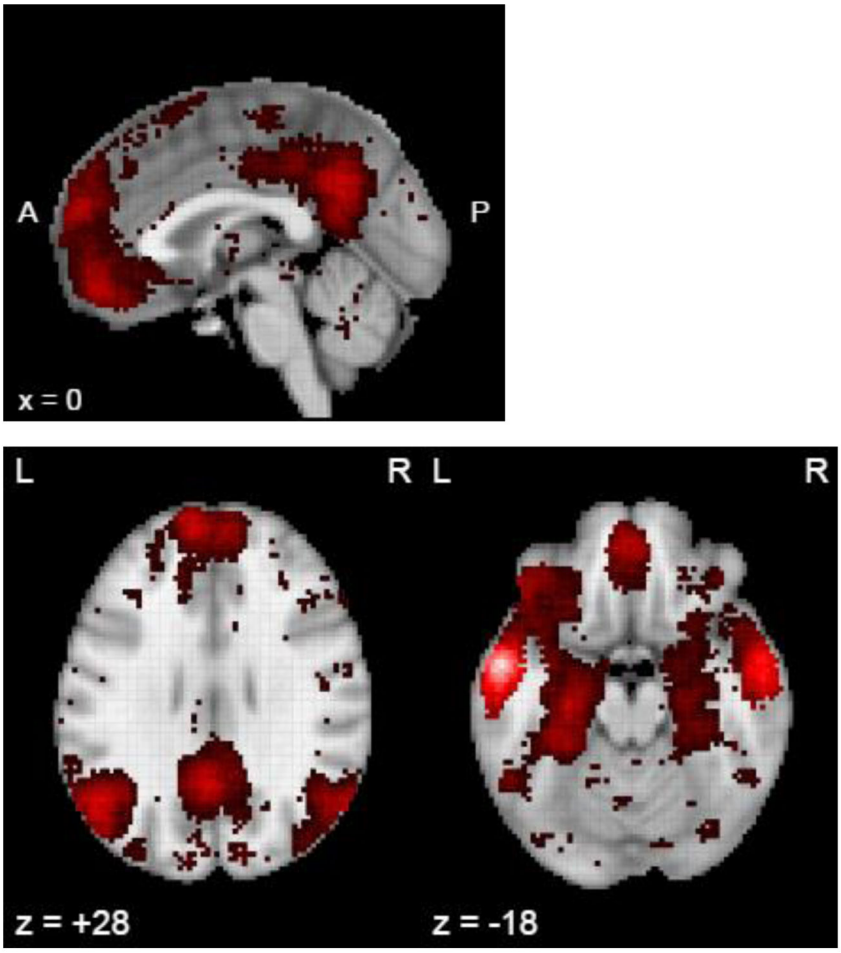

B

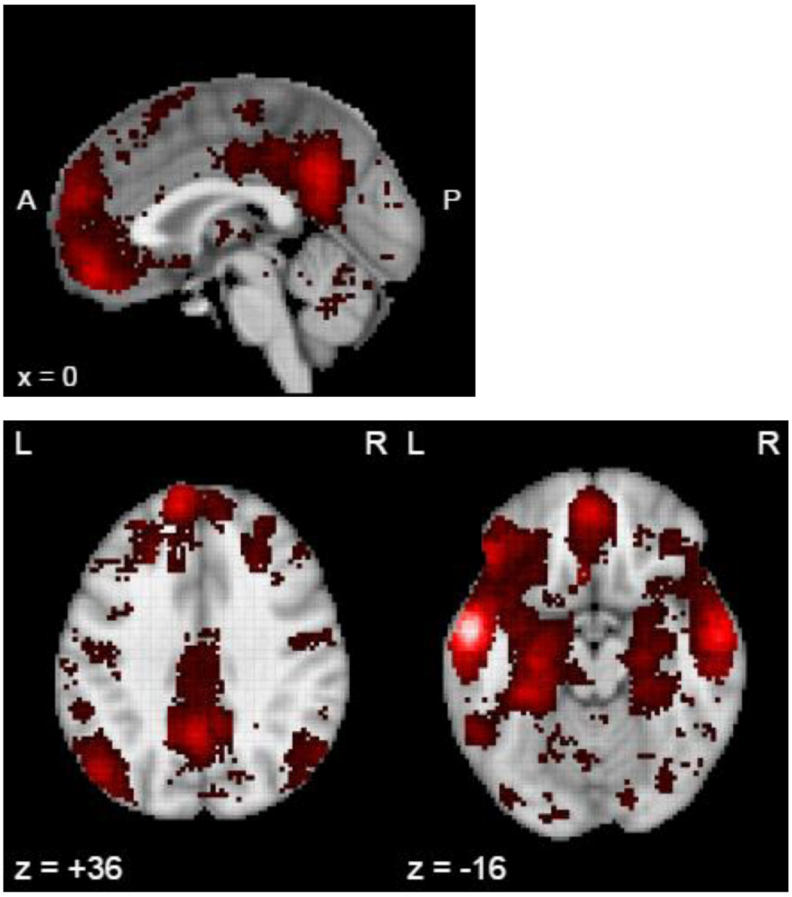

C

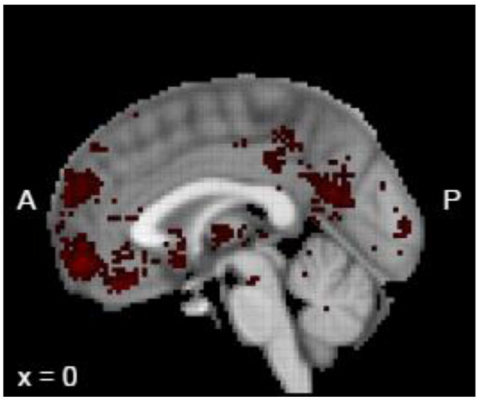

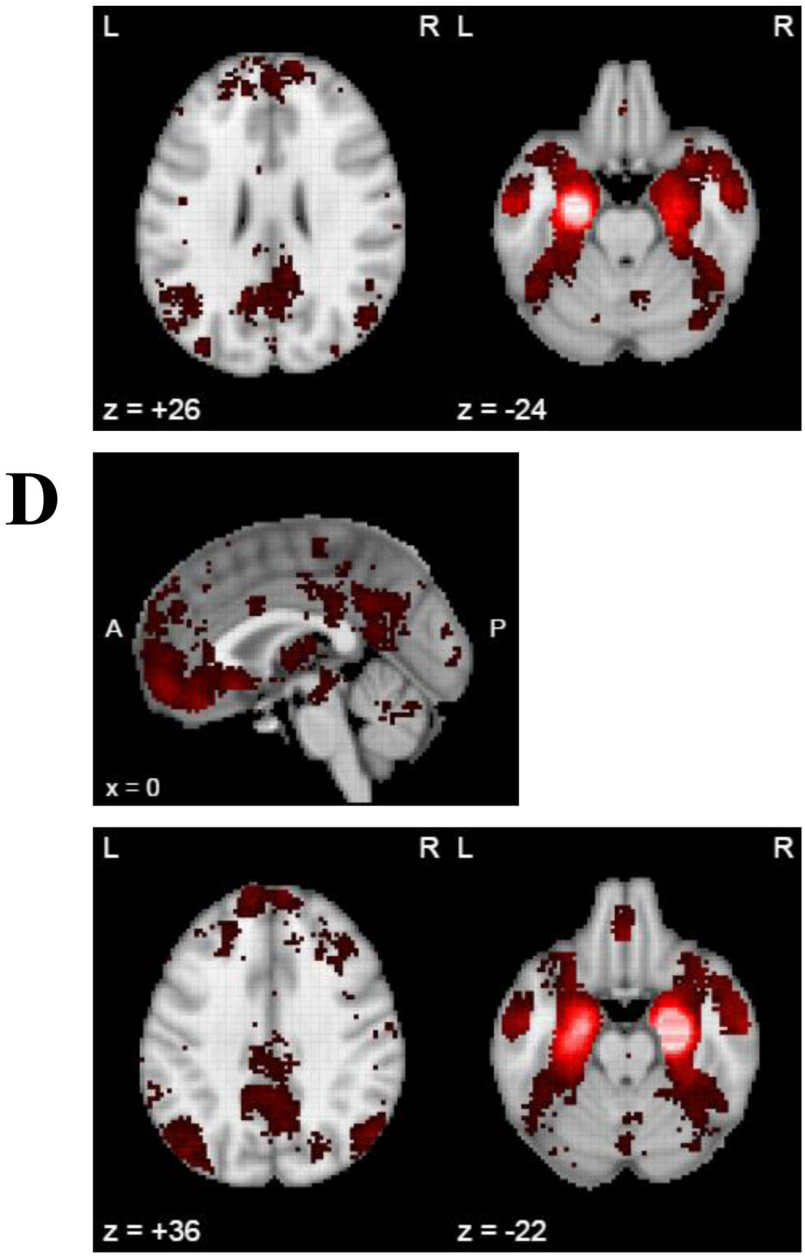

Figure 4.

Neurosynth co-activation meta-analysis of MTG and EC, thresholded at false discovery rate criterion of $p < .05$. Neurosynth had 11,406 studies, 150,000 brain locations, and 413,429 activations at time of analysis (April 18th, 2017). Red activation represents positive co-activation with seed region (white corresponds with the seed). No negative co-activation was found in any of the analyses completed. Maps show co-activation of the following seed regions: A) left middle temporal gyrus; B) right middle temporal gyrus; C) left entorhinal cortex D) right entorhinal cortex.

Table 1

Partial correlations of a gray matter volume in segmented regions (based on Desikan atlas) with area under the curve controlling for gender, age, income, and total intracranial volume. Only regions with significant p-values after FDR are included ($p < .05$).

Rank	Hemi	Region	*R*	*p*
1	L	Entorhinal Cortex	.151	1E-7
2	R	Middle Temporal Gyrus	.141	1E-6
3	L	Middle Temporal Gyrus	.140	1E-6
4	R	Entorhinal Cortex	.125	.1E-5
5	R	Fusiform Gyrus	.107	.001
6	L	Lateral Occipital Cortex	.101	.001
7	R	Inferior Temporal Gyrus	.098	.002
8	L	Precentral Gyrus	.098	.002
9	L	Postcentral Gyrus	.095	.002
10	L	Precuneus	.094	.003
11	L	Inferior Temporal Gyrus	.089	.004
12	R	Banks of Superior Temporal Sulcus	.087	.005
13	L	Lateral Orbitofrontal Cortex	.087	.005
14	R	Lateral Orbitofrontal Cortex	.086	.006
15	L	Insula	.083	.008
16	L	Transverse Temporal Cortex	.082	.008
17	R	Superior Frontal Gyrus	.080	.010
18	L	Temporal Pole	.079	.011
19	R	Parahippocampal Gyrus	.077	.014
20	R	Precentral Gyrus	.075	.016

Table 2

Final regression model of parcellation regions of interest as predictors of mean area under the curve. Model 1 R^2 = .035, p = 2E-7; Model 2 R^2 = .077, p = 1E-10. Significant variables are in boldface.

	Independent Variables	β	*t*	*p*
Model 1	Sex	.06	1.42	.16
	Age	−.04	1.27	.21
	Income	**.13**	**4.03**	**6E-5**
	Total Intracranial Volume	**.14**	**3.57**	**3E-4**
Model 2	**Bilateral Middle Temporal Gyrus**	**.20**	**4.363**	**1E-5**
	Bilateral Entorhinal Cortex	**.16**	**4.504**	**7E-6**

Dependent Variable: mean area under the curve for DRD of $200 and $40,000 USD.

Table 3

Summary of clusters in voxelwise analysis of gray matter volume. Coordinates of peak significance provided in Montreal Neurological Institute space (X Y Z). CWP = cluster-wise p-value.

Left Hemisphere Volume	**Size (mm^3)**	**X**	**Y**	**Z**	**CWP**
Anterior Middle Temporal Gyrus	799.26	−55.7	−2.1	−29.4	2E-5
Lingual Gyrus	255.96	−14.9	−69	−3.3	.010
Entorhinal Cortex	252.97	−25.5	−13.9	−32.6	.010
Lateral Occipital Cortex	228.65	−44.6	−81.5	2.9	.020
Right Hemisphere Volume	**Size (mm^3)**	**X**	**Y**	**Z**	**CWP**
Fusiform Gyrus	181.4	32.8	−33.9	−23.2	.040
Entorhinal Cortex	185.36	23.1	−14	−30.4	.040
Anterior Middle Temporal Gyrus	335.98	57.7	−1.8	−26.8	.002
Precentral Gyrus	285.7	41.5	3.5	25.7	.004
Posterior Middle Temporal Gyrus	217.85	62.6	−42.6	−3.9	.020

Table 4

Demographic characteristics of sample (N = 1038)

DEMOGRAPHIC CHARECTERISTIC	M (SD) or %
Sex	
Male	45.3%
Female	54.7%
Age	28.86 (3.69)
Race	
White or Caucasian	75%
Black or African American	14.7%
Asian American, Native Hawaiian, or other Pacific Islander	5.7%
Native American	.2%
More than one race	2.6%
Not sure or unknown	1.8%
Ethnicity	
Hispanic or Latino	8.4%
Not Hispanic or Latino	90.4%
Not sure or unknown	1.3%
Income	
$1,000–$9,999/year	7.2%
$10,000–$19,999/year	7.7%
$20,000–$29,999/year	11.9%
$30,000–$39,999/year	12.1%
$40,000–$49,999/year	10.3%
$50,000–$74,999/year	20.9%
$75,000–$99,999/year	13.8%
$100,000–$149,999/year	16.0%
Years of Education	14.94 (1.80)